A two-surface thermomechanical plasticity model considering thermal cyclic behavior

Wei Cheng, Ren-Peng Chen, Peng-Yun Hong, Yu-Jun Cui, Jean-Michel Pereira

A two-surface thermo-mechanical plasticity model considering thermal cyclic behavior

Wei Cheng[1], Ren-peng Chen[2], Peng-yun Hong[3], Yu-jun Cui[4], Jean-Michel Pereira[5]

[1] Ph.D candidate, Department of Civil Engineering, Zhejiang University, Hangzhou 310058, China, wcheng@zju.edu.cn

[2] Professor, Department of Civil Engineering, Zhejiang University, Hangzhou 310058, China; College of Civil Engineering, Hunan University, Changsha 410082, China; chenrp@zju.edu.cn, chenrp@hnu.edu.cn

[3] Former Ph.D student, Université Paris-Est, Laboratoire Navier (UMR 8205), CNRS, ENPC, IFSTTAR, F-77455 Marne-la-Vallée, France

[4] Professor, Université Paris-Est, Laboratoire Navier (UMR 8205), CNRS, ENPC, IFSTTAR, F-77455 Marne-la-Vallée, France

[5] Professor, Université Paris-Est, Laboratoire Navier (UMR 8205), CNRS, ENPC, IFSTTAR, F-77455 Marne-la-Vallée, France

Abstract

In thermal-related engineering such as thermal energy structures and nuclear waste disposal, it is essential to well understand volume change and excess pore water pressure buildup of soils under thermal cycles. However, most existing thermo-mechanical models can merely simulate one heating-cooling cycle and fail in capturing accumulation phenomenon due to multiple thermal cycles. In this study, a two surface elasto-plastic model considering thermal cyclic behavior is proposed. This model is based on the bounding surface plasticity and progressive plasticity by introducing two yield surfaces and two loading yield limits. A dependency law is proposed by linking two loading yield limits with a thermal accumulation parameter n_c, allowing the thermal cyclic behavior to be taken into account. Parameter n_c controls the evolution rate of the inner loading yield limit approaching the loading yield limit following a thermal loading path. By extending the thermo-hydro-mechanical equations into the elastic-plastic state, the excess pore water pressure buildup of soil due to thermal cycles is also accounted. Then, thermal cycle tests on four fine-grained soils (natural Boom clay, Geneva clay, Bonny silt and reconstituted Pontida clay) under different OCRs and stresses are simulated and compared. The results show that the proposed model can well describe both strain accumulation phenomenon and excess pore water pressure buildup of fine-grained soils under the effect of thermal cycles.

Keywords: fine-grained soils; strain accumulation; thermal cycles; two-surface model; excess pore water pressure buildup

1. Introduction

Around energy piles [1-3], nuclear waste canisters [4], buried tunnels and pipes [5], the soils suffer from temperature effects, especially heating-cooling cycles. Observations of different fine-grained soils in the laboratory and in the field [6-11] showed that heating generally induced non-negligible volume change and excess pore water pressure buildup. Several thermo-mechanical models were proposed to describe this thermo-mechanical behavior of fine-grained soils [13-21]. Some of them extended the Cam-clay or modified Cam-clay model to the temperature effect by introducing a shrinking yield surface [13-17]. These models could describe some basic thermo-mechanical behavior, but fail to describe the soil behavior in over-consolidated states. In order to well describe the small thermo-mechanical elastic zone and the shear softening behavior, some advanced models consider two yield surfaces based on the bounding surface theory [18-21]. Hong et al. [22] made a comparison among some of these advanced models, and showed that the multiple plastic hardening mechanism were of paramount importance in modeling complex thermal loading behavior.

Though numerous efforts were made in thermal mechanical modeling, most existing models can only simulate the case of one thermal cycle and fail in describing the soil behavior under multiple heating-cooling cycles. As more attention has been paid to the long-term performance [11,12,25,26,27,40], the volume change and excess pore water pressure accumulation due to temperature variation can act as a significant factor influencing the safety of energy structures. Demars and Charles [23] reported a series

of drained thermal cycle tests on high plastic marine clays and found that permanent reduction in void ratio (a function of over-consolidation ratio) gradually reduced due to temperature cycles (see Fig.1). Plum et al. [24] conducted an undrained heating-cooling cycle tests on Newfield clay. After four thermal cycles, the accumulation of excess pore water pressure was still increasing. Pastén et al. [40] experimentally observed the thermally driven displacement accumulation with the number of temperature cycles and developed a thermally induced ratcheting mechanism for a smooth interface. All those observations show that multiple thermal cycles should be considered in thermal mechanical modeling of clays. Zhou et al. [28] recently proposed a bounding surface model with a memory surface to consider the thermal cyclic behavior. However, this imposed memory surface actually has no effect on the accumulation behavior of normally consolidated soil because this memory surface coincides with the bounding surface in this circumstance. Ma et al. [29] proposed a thermal stabilization line in hypoplastic modeling approach. Though three thermal parameters are introduced, the proposed hypoplastic model fails to describe the strain accumulation during relatively small temperature changes because it always simulates an unrealistic elastic behavior before entering the elasto-plastic zone following a thermal loading path. More recently, Zymnis et al. [41] proposed a simple calibration procedure for Tsinghua ThermoSoil (TTS) model and studied the capabilities of simulating the long-term accumulation of strains due to thermal cycles. However, those existing models for thermal cyclic behavior merely considered the strain accumulation behavior under drained conditions

85 though the excess pore water pressure buildup due to temperature effects are at least of
86 equal importance from the best of the authors' knowledge.
87 In the present work, a two surface thermo-plastic model, namely ACC2-T, is
88 proposed to consider the thermal cyclic behavior based on the previous TEAM model
89 by Hong et al. [21]. The proposed model unifies the loading yield limits and the thermal
90 yield limits. To connect the inner loading yield limit and the loading yield limit, a
91 flexible dependency law is incorporated and combined with isotropic and progressive
92 hardening laws to account for multiple thermal cycles. In the dependency law, a
93 parameter n_c is introduced to control accumulation rate through the evolution rate of the
94 inner loading yield limit approaching the loading yield limit. Meanwhile, the proposed
95 model is extended to undrained condition by applying the thermo-hydro-mechanical
96 equations by Coussy [30] into the elastic-plastic state. Then, the rationale of ACC2-T
97 model is discussed in terms of elasto-plasticity and thermodynamic theories. Lastly, the
98 thermal cycle test results of four fine-grained soils (natural Boom clay, Geneva clay,
99 Bonny silt and reconstituted Pontida clay) under different OCRs and stresses are used
100 to verify the proposed model.
101

102 2. Model description

103 In this section, the proposed model (ACC2-T) is presented using typical constitutive
104 variables, namely mean effective stress p', deviator stress q, temperature T and the
105 corresponding increments (dp', dq, dT). The soil behavior is assumed to be isotropic

and the constitutive model is developed and formulated in the conventional triaxial conditions.

2.1 Thermo-elastic behavior

In ACC2-T model, the soil deformation can be divided into thermo-elastic and thermo-plastic parts.

In the thermo-elastic part, the elastic law adopted in many other models [31,36,37] in isothermal conditions are extended into non-isothermal conditions for its simplicity. the total elastic volumetric strain increment associated with mechanical and thermal loading and the elastic shear strain assumed purely mechanical are calculated as follows:

$$d\varepsilon_v^e = \frac{\kappa dp'}{\upsilon p'} - \alpha_1 dT\,,\ d\varepsilon_s^e = \frac{dq}{3G},\ G = \frac{3(1-2v)}{2(1+v)}\frac{\upsilon p'}{\kappa} \tag{1}$$

where $d\varepsilon_v^e$, $d\varepsilon_s^e$ is the elastic volumetric strain increment ($d\varepsilon_v^e = d\varepsilon_1^e + d\varepsilon_2^e + d\varepsilon_3^e$) and the elastic shear strain increment ($d\varepsilon_s^e = \frac{2}{3}\left(d\varepsilon_1^e - d\varepsilon_3^e\right)$). κ is the elastic slope in (υ, ln p') plane and υ is the specific volume. α_1 is the thermal elastic compressibility index which assumed a positive constant because heating induces soil expansion. G is shear modulus and v is the Poisson's ratio.

2.2 Thermo-plastic behavior

The thermo-plastic mechanism of ACC2-T model consists of two yield surfaces and plastic potential surface, the dependency law, the isotropic and progressive hardening

126 laws and the flow rules.

127

128 *2.2.1 Yield surfaces and plastic potential surfaces*

129 In ACC2-T model, two yield surfaces, namely loading surface (f_l) and yield surface (f_Y),

130 with a generalized formulation [31] are implemented to model the yielding of both stiff

131 and soft clays.

132 Loading Surface: $$f_l = q^2 + \frac{M_f^2}{1-k_f}\left(\frac{p'}{r\bar{p}'_{cT}}\right)^{\frac{2}{k_f}}\left(r\bar{p}'_{cT}\right)^2 - \frac{M_f^2 p'^2}{1-k_f} = 0 \quad (2)$$

133 Yield Surface: $$f_Y = q^2 + \frac{M_f^2}{1-k_f}\left(\frac{p'}{\bar{p}'_{cT}}\right)^{\frac{2}{k_f}}\bar{p}'^{\,2}_{cT} - \frac{M_f^2 p'^2}{1-k_f} = 0 \quad (3)$$

134 where M_f is the stress ratio at the apex of two surfaces, k_f is a parameter specifying the

135 shape of yield surfaces, $\bar{p}'_{cT}$ is the pre-consolidation pressure at current temperature T

136 and r is the inverse of over-consolidation ratio (OCR) at current temperature T. The

137 conceptual plot of two yield surfaces at various temperature is given in Fig. 2(a). To

138 consider the thermo-mechanical behavior, the two surfaces are extended into three-

139 dimensional plot (p', q, T) with two loading yield limits. The two loading yield limits,

140 namely the inner loading yield limit (*ILY*) and the loading yield limit (*LY*) are linked by

141 the proposed dependency law which is discussed in *Yield limits and dependency law*

142 section.

143 The plastic potential surface g_l takes the same form as for loading surface, but with

144 different parameters M_g and k_g:

$$g_I = q^2 + \frac{M_g^2}{1-k_g}\left(\frac{p'}{r\beta}\right)^{\frac{2}{k_g}}\left(r\beta\right)^2 - \frac{M_g^2 p'^2}{1-k_g} = 0 \tag{4}$$

and it leads to a dilatancy equation in the case of triaxial compression:

$$\frac{d\varepsilon_v^p}{d\varepsilon_s^p} = \frac{\frac{\partial g_I}{\partial p'}}{\frac{\partial g_I}{\partial q}} = \frac{M_g^2 - \eta^2}{k_g \eta} \tag{5}$$

where $d\varepsilon_v^p$ is the plastic volumetric strain increment, $d\varepsilon_s^p$ is the plastic shear strain increment, η denotes the stress ratio q/p', M_g defines the critical stress ratio at failure where no further volumetric strain increment develops, k_g is a constant parameter which controls the ratio of plastic volumetric strain increment and plastic shear strain increment and β is the size parameter. Typically, an unassociated flow rule is adopted for modeling complex mechanical behaviors. However, when $M_g = M_f$ and $k_g = k_f$, an associated flow rule would be recovered. When $k_g = k_f = 2$, elliptical surfaces like modified Cam-clay model are recovered.

2.2.2 Hardening laws

In ACC2-T model, two plastic hardening mechanisms fixed to reference temperature T_0 are adopted to control the evolution of yield surface and loading surface.

In the isotropic hardening rule, as same as in Modified Cam-clay model, the evolution of pre-consolidation pressure $\overline{p}'_{c0}$ at reference temperature T_0 is linked to the plastic volumetric strain increment:

$$d\overline{p}'_{c0} = \frac{\upsilon}{\lambda - \kappa}\overline{p}'_{c0} d\varepsilon_v^p \tag{6}$$

where λ is the normal consolidation slope in (υ, ln p') plane and $d\bar{p}'_{c0}$ is the increment of pre-consolidation pressure. It means the evolution of yield surface is dominated by the plastic volumetric strain.

The progressive hardening variable dr_0, at reference temperature T_0, is defined with a combined volumetric and shear plastic strain as follows:

$$dr_0 = \frac{\upsilon}{\lambda - \kappa} s\left(1 - r_0\right)\left(d\varepsilon_v^p + A_d d\varepsilon_s^p\right) \tag{7}$$

where r_0 is the inverse of over-consolidation ratio (OCR) at current temperature T_0 and dr_0 is the increment. s is a material constant which controls the hardening rate of loading surface in approaching yield surface. A_d is a material constant which controls the contribution of shear plastic strain.

In this progressive hardening rule, parameter r_0 is always less than or equal to 1 ($0 < r_0 \leq 1$). When the loading surface is completely inside the yield surface ($0 < r_0 < 1$), it means the soil is over-consolidated. Within the hardening process, plastic strain increases and the loading surface begins to move towards the yield surface ($dr_0 > 0$). When $r_0 = 1$, the loading surface and the yield surface coincide. The soil turns into normally consolidated state as the same case of MCC model. Note that the loading surface could not run out of the yield surface ($r_0 > 1$) for the fact that if $r_0 > 1$, $dr_0 < 0$ holds. With such a combined volumetric-deviatoric hardening law, the inclusion of shear hardening part ($d\varepsilon_s^p > 0$) would lead to a positive plastic modulus ($h > 0$) even when the effective stress state ($d\varepsilon_v^p = 0$) reach the critical state line (CSL). As a consequence, the stress point lying on the loading surface can cross the CSL,

185 hardening continues to a stress point ($d\varepsilon_v^p < 0,\ \ d\varepsilon_s^p > 0, h = 0$) and then the stress point
186 ($d\varepsilon_v^p < 0,\ \ d\varepsilon_s^p > 0,\ h < 0$) would move back to the CSL. This approach allows to
187 predict shear softening behavior and it is often the case of highly over-consolidated
188 states of soil.

189 With these isotropic and progressive hardening rules, the plastic modulus and
190 increment stress-strain relationship of ACC2-T model are obtained in Appendix A.

191 Under loading and heating processes, two hardening variables $\overline{p}'_{c0}$ and r_0 are
192 activated with the evolution of plastic strain. However, under unloading and cooling
193 processes, pure elastic strain develops with a fixed value of $\overline{p}'_{c0}$. Due to ACC2-T model
194 strictly adhering to the principle that the stress point is always lying on the loading
195 surface, the value of r_0 could be re-calculated by a simple Newton-Raphson Method
196 with unconditional stability.

197

198 *2.2.3 Yield limits and dependency law*

199 In the two surface models, the loading surface and the yield surface are geometrically
200 similar in (p', q) plane with a corresponding radial mapping rule. In previous TEAM
201 model [21], two yield limit mechanisms, namely thermal yield limits (*ITY*, *TY*) and
202 loading yield limits (*ILY*, *LY*) are adopted to model the thermal behavior. These yield
203 limit mechanisms in TEAM model (see Fig.3(a)) enable the thermal elastic response in
204 reloading path to occur before entering the elasto-plastic zone. Therefore, the TEAM
205 model could not simulate the strain accumulation phenomenon due to temperature

206 variations. In order to overcome this shortcoming and extend the model to the case of
207 multiple thermal cycles, the loading yield limits (*ILY*, *LY*) are unified to consider both
208 the thermal yield and loading yield mechanisms. Meanwhile, a new dependency law is
209 proposed to connect *ILY* and *LY*.

210 In the dependency law, the pre-consolidation pressure $\bar{p}'_{cT}$ at current temperature *T*
211 takes the original form and it would decrease with the increase of temperature:

212 $$\bar{p}'_{cT} = \bar{p}'_{c0} \exp\left[-\alpha_0(\mathrm{T}-\mathrm{T}_0)\right] \tag{8}$$

213 where $\bar{p}'_{c0}$ is pre-consolidation pressure at reference temperature T_0; α_0 is a material
214 constant controlling the thermal plastic behavior.

215 The other part of the dependency law *r* is defined as below:

216 $$r = \frac{1}{OCR} = \frac{p'}{\bar{p}'} = \frac{q}{\bar{q}} = \frac{p'_{cT}}{\bar{p}'_{cT}} \tag{9}$$

217 where (p', q), ($\bar{p}'$, $\bar{q}$) is the corresponding stress point in loading surface and yield
218 surface at current temperature *T*, respectively.

219 Unlike TEAM model with the assumption that $r = r_0$, ACC2-T model takes the form
220 that would make *ILY* not necessarily homologous to *LY* any longer (see Fig.3(b)):

221 $$r = r_0 \exp\left[-\alpha_0(r_0^{n_c} - 1)(\mathrm{T}-\mathrm{T}_0)\right] \tag{10}$$

222 where n_c is a thermal parameter which controls the strain accumulation rate under
223 multiple thermal cycles.

224 The combined dependency law made up by $\bar{p}'_{cT}$ and *r* then is expressed by:

225 $$r\bar{p}'_{cT} = r_0\bar{p}'_{c0} \exp\left[-\alpha_0 r_0^{n_c}(\mathrm{T}-\mathrm{T}_0)\right] \tag{11}$$

226 In the proposed law, the shape of *ILY* is governed by the key thermal accumulation

227 parameter n_c. Parameter n_c controls the evolution rate of *ILY* approaching *LY* by the two
228 isotropic and progressive hardening rules. In order to illustrate the plastic mechanism
229 under the thermal path, two cases in the isotropic states, namely $n_c < 0$ and $n_c = 0$, are
230 compared in Fig.4. Both two cases are at initial stress state A, then heated up to stress
231 state B and finally cooled down to stress state A. Under the heating path from A to B,
232 the *ILY* without n_c ($n_c = 0$) would induce a increment of Δr_1. For the case of $n_c < 0$, it
233 would induce a increment of $\Delta r_1 + \Delta r_2 + \Delta r_3$ if the shape of *ILY* is fixed. However, with
234 the effect of n_c, the original *ILY* (see Fig.4(b), dotted line I) would gradually turn into
235 solid line II with a actual increment of $\Delta r_1 + \Delta r_2$. The larger increment $\Delta r_1 + \Delta r_2$ in
236 hardening variable dr_0 would mean larger plastic volumetric strain increments than the
237 case of $n_c = 0$. Under the cooling path from B to A, the mechanical response is purely
238 elastic and the shape of *ILY* would turn from II into I. For the case of $n_c > 0$, the
239 increment in hardening variable dr_0 would induce smaller strain increments than $n_c = 0$.
240 Under multiple thermal cycles, the value of r_0 would be smaller and smaller.

241 Under such a unique dependency law, the evolution rate of *ILY* is actually the
242 evolution rate of strain accumulation. With a proper selection of parameter n_c in the
243 dependency law, ACC2-T model allows the strain accumulation under the effect of
244 multiple thermal cycles to be modelled. Some important features about the dependency
245 law and parameter n_c are summarized below:

246 1. When the current temperature T is equal to the reference temperature T_0, r becomes
247 equal to r_0. It means that n_c would have no effect on the stress-strain relationship at

reference temperature T_0.

2. When soil turns into the normal consolidated state ($r_0 = 1$), r is also equal to 1. In that case, *ILY* would coincide with *LY*. It means that n_c would have no effect on the behavior of normal consolidated soils under either isothermal or non-isothermal condition.

3. When n_c is equal to zero (bold line in Fig. 3(b)), r becomes equal to r_0. In that case, a similarity between *ILY* and *LY* would be recovered. This is just the case of *ILY* and *LY* used in TEAM model [21].

4. Theoretically, the value of n_c can be chosen from negative infinity to positive infinity. When n_c tends to positive infinity, *ILY* would tend to be the dotted line in Fig. 3(b). When n_c tends to negative infinity, *ILY* would tend to approach the temperature axis T in Fig. 3(b). A larger n_c represents a quicker strain accumulation rate which would induce smaller total volumetric strain accumulation under the effect of thermal cycles.

5. Any possible r is smaller than 1. During the heating process, the hardening mechanism enables r_0 to approach 1. Thus, r would also have its limit value of 1 which implies that the over-consolidation ratio of soil is always larger than or equal to 1.

3. Loading path independence

After the description of the proposed model extended to thermal cyclic behavior, it is essential to discuss the rationale of ACC2-T model in terms of elasto-plastic theory and thermodynamic theory as Hong et al. [22] did on three existing thermo-mechanical models [19,20,25,28,29]. The verification of loading path independence is made up by

both the thermo-elastic and thermo-plastic part. The schematic plot is given in Fig.5. Heating is treated as a special isotropic loading. Therefore, merely isotropic condition ($q=0$) is considered during the derivation. The thermo-elastic part is discussed as below and the derivation in thermo-plastic regime is attached in Appendix B.

In the thermo-elastic mechanism (Eq.3) of ACC2-T model, the bulk modulus $K=\frac{\upsilon p'}{\kappa}$ is independent of temperature, and thermal elastic compressibility index α_1 is also independent of mean effective stress. Such elastic volumetric strain in ACC2-T model is surely loading path independent in (p', T) plane. Note that the thermo-elastic mechanism leads to loading path dependent in (p', q) plane since the Maxwell symmetry relations are not satisfied. A possible way is to extend a hyperelastic law [39] into non-isothermal conditions. For simplicity of parameter calibration, merely this thermo-elastic mechanism is considered here.

4. Analysis and determination of model parameters

The proposed ACC2-T model contain fifteen parameters (λ, κ, $\overline{p}'_{c0}$, v, M_f, k_f, M_g, k_g, s, r_0, A_d, α_0, α_1, T_0, n_c). Five of them (λ, κ, $\overline{p}'_{c0}$, v, M_g) are commonly defined in MCC model. (M_f, k_f), (M_g, k_g) control the shapes of yield surfaces and plastic potential surfaces, respectively. Three parameters (s, r_0, A_d) are used to consider a progressive yielding of two surfaces. Four parameters (α_0, α_1, T_0, n_c) are defined to consider the thermal influence on the soil behavior. The procedure for determining these parameters is described and key parameters (λ, κ, $\overline{p}'_{c0}$, s, r_0, α_0, α_1, T_0, n_c) related to thermal

accumulation behavior are discussed on the set of model parameters for natural Boom clay in Fig. 6.

1. By an isotropic compression test or oedometer test under reference temperature T_0, κ, λ, the initial $r_{0,0}$ and $\overline{p}'_{c0,0}$ are determined in (υ, ln p') plane in Fig.6(1). Note that parameter s controls the hardening rate of loading surface in approaching yield surface. It can be determined by fitting nonlinearity from over-consolidated states to normal consolidated state in (υ, ln p') plane.

2. By an isotropic heating-cooling test at normally consolidated states, α_1 is determined by fitting data of cooling stage and α_0 is determined by the heating test in (T, $\Delta\varepsilon_v$) plane in Fig.6(2).

3. By a continuous thermal cycle test, the volumetric strain increment by each thermal cycle $\Delta\varepsilon_{v,st}$ can be obtained ($\Delta\varepsilon_{v,st}$, n) plane in Fig.6(3). The thermal accumulation parameter n_c, which controls the strain accumulation rate, is then determined by calibrating the strain accumulation under each thermal cycle.

4. M_f, k_f. M_f denotes the apex of yield surface and k_f controls the shape of yield surface. They are calibrated by fitting the converntional yield points of various stress paths.

5. M_g is the critical state stress ratio and it is calibrated by the effective stress ratio at critical state.

6. k_g controls plastic flow direction. It is determined by fitting the values of $d\varepsilon_v^p / d\varepsilon_s^p$ in drained triaxial shear tests.

7. The poisson's ratio v is determined by a triaxial tests at low strain level in the (ε_v-ε_1)

311 plane: $v = (\varepsilon_v - \varepsilon_1)/2$.

312 *8.* A_d represents the contribution of the plastic shear strain in the hardening process. It
313 is calibrated by fitting the results of triaxial compression tests at over-consolidated
314 states in (q, ε_1) or (ε_v, ε_1) plane in Fig.6(4).

315

316 # 5. Model Validation and prediction

317 In this section, four different fine-grained soils, namely natural Boom clay, Geneva clay,
318 Bonny silt and reconstituted Pontida clay, are adopted to verify the capability of ACC2-
319 T model in modeling the thermal cyclic behavior.

320

321 ***5.1 Natural Boom clay***

322 One heating and cooling test on natural Boom clay (I_p = 31) under isotropic stress
323 states performed by Baldi et al. [8] and two groups of triaxial compression tests
324 conducted by Lê [38] are taken into account.

325 In the heating and cooling test, specimen TBoom-9 taken from Mol at an in-situ depth
326 of 223 m (initial pre-consolidated pressure of 6 MPa) is tested under a mixed
327 mechanical and thermal loading process: the sample was firstly saturated under a
328 constant mean effective stress of 2 MPa at 21.5 °C, loaded up to 4 MPa, unloaded to 1
329 MPa, heated up to 95 °C and cooled back to 21.5 °C, loaded up to 3 MPa at 21.5 °C
330 and heated up to 95 °C and cooled back, loaded up to 6 MPa and heated up again and
331 finally cooled back. In the loading process, three thermal cycles of temperature

increment of 73.5 °C at different isotropic stress states, namely mean effective stress of 1 MPa, 3 MPa and 6 MPa, are selected for simulation. For better comparison between the computed and measured results, the increments of volumetric strain are reset at the starting point of each heating-cooling cycle. Moreover, Fig. 7 contains an isotropic compression test of natural Boom clay from 2 MPa to 20 MPa, then back to 6 MPa. Basic parameters for natural Boom clay are listed in Tab.1.

The TEAM model [21] and the proposed ACC2-T model are both used for simulation in Fig.8. It appears that both models can describe the thermal volume change well for normally consolidated or slightly over-consolidated state (p' = 6 MPa) adopting the same thermal elastic parameter α_1 and thermal plastic parameter α_0. However, for highly over-consolidated states (p' = 3 MPa, p' = 1 MPa), it is observed that ACC2-T model gives a more consistent simulation than TEAM model. One reason is that TEAM model always shows a linear elastic expansion behavior before entering the elasto-plastic zone and has no parameters controlling strain evolution. With this shortcoming, TEAM model would fail to respond to thermal cycles and thus to describe strain accumulation behavior, though complicated multiple plastic mechanisms are adopted. However, in ACC2-T model, the stress point is always lying on the loading surface. Combined with the isotropic and progressive hardening rules, the thermal accumulation parameter n_c in the dependency law allows the ACC2-T model to better describe the nonlinear expansion behavior and strain accumulation under over-consolidated states. Meanwhile, as natural Boom clay is relatively easy to contract under heating, the use

353 of a negative value of parameter n_c could facilitate the simulation of such aspect.

354 In the triaxial compression test, the experimental results of drained triaxial
355 compression tests ($p_0' = 2.5$ MPa, $p_0' = 4$ MPa) at room temperature 25 °C and drained
356 triaxial compression tests ($p_0' = 2.5$ MPa, $p_0' = 3.8$ MPa) at high temperature 76 °C
357 [38] are considered in (q, ε_1)plane and (ε_v, ε_1) plane in Fig.9. In these moderate over-
358 consolidated states, the shear strength at room temperature is a bit higher than high
359 temperture. However, a larger volumetric strain is generated at high temperature than
360 room temperature as shown in (ε_v, ε_1) plane. At the same time, the smooth predictions
361 by ACC2-T model agree well with the experimental observations. Two values of n_c (n_c
362 = -1, n_c = 0) are selected to simulate the behaivor at high temperature 76 °C. It indicates
363 that the value of n_c has a negligible effect on the prediction of triaxial tests.

364 A numerical case at high over-consolidated state ($p_0' = 0.5$ MPa) under both two
365 temperatures (25 °C, 76 °C) are conducted. A slight shear dilatancy is predicted at axial
366 strain of about 5%. However, the post-peak softening phenomenon in (q-ε_1) plane is not
367 very apparent because parameter A_d (A_d = 0.1) for natural Boom clay is very small to
368 simulate behaviors at both high, slightly over-consolidated and normal consolidated
369 states.

370

371 ***5.2 Geneva clay***

372 Multiple thermal cycles were applied on Geneva clays (I_p = 11.1) in a temperature-
373 controlled oedometer cell under drained condition [25]. A normally consolidated soil

374 sample with a vertical effective stress of 125 kPa was tested with four temperature
375 cycles from 5 °C from 60 °C, starting at a room temperature of 20 °C. The one-
376 dimension test results are simulated in Fig.7 and the calibrated model parameters are
377 listed in Tab.1.

378 Fig.10 shows the measured and computed soil behavior under multiple heating and
379 cooling cycles. The computed result of ACC2-T model (Fig.10(a)) shows a good
380 agreement with the measured one. The irreversible volumetric strain accumulates with
381 increasing thermal cycles, but at a decreasing rate (Fig.10(c)). The value of 3.5 is shown
382 appropriate for the thermal accumulation parameter n_c to control the strain
383 accumulation rate. For the case of TEAM model, the computed result of first thermal
384 cycle is the same as ACC2-T model. However, the response of TEAM model is purely
385 elastic thereafter and the thermal strain accumulation could not be described. In
386 Fig.10(b), a sensitivity analysis of ACC2-T model is conducted to study the effect of
387 parameter n_c on the strain accumulation. Two other n_c values of 0, 10 are selected for
388 this purpose. In the first thermal cycle, ACC2-T model gives the same results for all the
389 three n_c values because the thermal volumetric strain of normally consolidated soil is
390 only dependent on thermal elastic parameter α_1 and thermal plastic parameter α_0.
391 From the second thermal cycle, the soil becomes over-consolidated. The thermal
392 accumulation parameter n_c starts to control the strain evolution rate. From Fig.10(c), it
393 appears that parameter n_c is positively correlated to the strain accumulation rate and a
394 proper selection of parameter n_c is crucial for total strain accumulation.

5.3 Bonny silt

Multiple heating and cooling cycles were applied on compacted Bonny silt (I_p = 4) under different OCRs in a temperature-controlled oedometer cell [27]. Bonny silts were first mechanically consolidated to a vertical effective stress of approximately 1200 kPa at a constant room temperature of 18 °C. Then, they were unloaded to reach five different OCR values of 1.00, 1.28, 1.80, 7.36 and 30.29. Fig. 7 presents the experimental and calibration results of one-dimensional test of Bonny silt. Four heating and cooling cycles were applied under drained condition with different OCRs in a temperature ranging from 18 ºC to 93 ºC.

It can be seen from Fig.11 that at slightly over-consolidated states (i.e. OCR = 1, 1.28 and 1.8), the measured and computed results show a good consistency. That means the thermal accumulation parameter n_c can properly control the strain evolution rate under various over-consolidated states. However, for highly over-consolidated ones (i.e. OCR = 7.36, 30.29) in the literature [27], the volumetric strain accumulation is quite small or even becomes negative, suggesting that the expansion and the contraction of the oedometer cell can be no longer ignored. These two samples are not considered in the simulation.

5.4 Reconstituted Pontida clay

The excess pore water pressure accumulation due to thermal cycles in validated by a heating and cooling test of reconstituted Pontinda clay. Hueckel et al [12] reported this measured and computed results on reconstituted Pontida clay. The reconstituted silty

clay sample was firstly loaded to a mean effective stress state of 2.5 MPa. Then it underwent a heating-cooling cycle from 22°C to 65°C and back to 22°C, then a continuous heating to 95°C in a constant total isotropic stress state.

Although some previous models [19] consider the undrained behavior by imposing a constant volume condition which is imprecise under non-isothermal conditions, the undrained computation using ACC2-T model is obtained by extending the energy and mass conservation of thermo-poro-elastic media into elasto-plastic states [30].

In a saturated porous media, the current water mass (m_w) per unit volume can be expressed as:

$$m_w = \rho_w \phi \tag{12}$$

where ρ_w is water density and ϕ is the Lagrangian porosity.

In undrained conditions, water mass is constant and $dm_w = 0$ holds, then

$$\frac{dm_w}{\rho_w} = d\phi + \phi \frac{d\rho_w}{\rho_w} = d\phi + \phi\left(C_w du - \alpha_w dT\right) = 0 \tag{13}$$

where α_w, C_w, is the water thermal expansion coefficient, water compressibility, respectively.

In isotropic stress state and under non-isothermal condition, total mean stress change (dp) and Lagrangian porosity change ($d\phi$) can be expressed with Maxwell's symmetry condition:

$$dp = \frac{1}{C_d} d\varepsilon_v + (1 - \frac{C_s}{C_d}) du_w + \frac{\alpha_d}{C_d} dT \tag{14}$$

$$d\phi = -(1 - \frac{C_s}{C_d}) d\varepsilon_v - (\phi - 1 + \frac{C_s}{C_d}) C_s du_w + (\phi - 1 + \frac{C_s}{C_d}) \alpha_s dT \tag{15}$$

where C_s, C_d, α_s, α_d is the volumetric compressibility coefficient of solid grain, the volumetric compressibility of soil skeleton, the thermal expansion coefficient of solid grain and the thermal expansion coefficient of soil skeleton. It is often the case that $\alpha_s = \alpha_d$.

Thus, the expressions for excess pore water pressure can be obtained, as follows:

$$d\varepsilon_v = -\left(\phi\alpha_w + \left(1-\phi\right)\alpha_s\right)dT + \phi\left(C_w - C_s\right)du_w + C_s dp \tag{16}$$

With infinitesimal transformation and clayey soils, the fact ($C_s \approx 0$, $n \approx \phi$) is commonly accepted. Thus

$$du_w = \frac{d\varepsilon_v + (n\alpha_w + (1-n)\alpha_s)dT}{nC_w} \tag{17}$$

where n is Eulerian porosity.

For reconstituted Pontida clay, α_s is 1×10^{-5} (1/°C) chosen as same as α_1, which is calibrated from an undrained cooling process from 65°C to 22°C. α_w and C_w are calibrated from a heating test of free water in the literature [35].

The computed results of excess pore water pressure by ACC2-T model and TEAM model are compared to the measured data and Hueckel's simulation [12] in Fig.12. It is seen that both predictions of ACC2-T model and TEAM model are more accurate than Hueckel's simulation, especially the existed buildup of pore water pressure in experimental results. During the heating stage from 22°C to 65°C, the mean effective stress will decrease with temperature (equivalent to a mechanical loading under undrained condition) and the effective stress-temperature path (T - p') initially enters plasticity. With the plastic hardening of *ILY*, excess pore water pressure is increased. Then during the cooling stage from 65°C to 22°C, the response is purely elastic with a decrease of the pore water pressure. Thereby, an irreversible excess pore water pressure is observed after one heating-cooling cycle which is well captured by ACC2-T model and TEAM model. Moreover, though the cooling stage is purely elastic, the *ILY* would shrink to make the stress-temperature state always lying on it. However, during the re-heating process, TEAM model could not build up excess pore water pressure from 22°C to 65 °C because the response is purely elastic. As for ACC2-T model, the clay sample is initially over-consolidated, then began to build up excess pore water pressure with the control of thermal accumulation parameter n_c in the whole process from 22°C to 95 °C.

5.5 Discussion

Four fine-grained soils are selected to verify the capability of ACC2-T model on modelling thermal cyclic behaviors under drained and undrained conditions. A thermal accumulation parameter n_c control the accumulation rate under multiple thermal cycles. Meanwhile, the values of n_c are ranked as: natural Boom clay< reconstituted Pontida clay<Geneva clay<Bonny silt. It means the clays, containing more clay contents, showing larger plastic index I_p, are more likely to accumulate volumatric strain and build up excess pore water pressure. Generally, the larger is the plastic index I_p, the smaller is the value of n_c. A liner regression function is obtained to evaluate the correlation between parameter n_c and plastic index I_p in Fig. 13.

6. Concluding remarks

A two-surface plasticity model (ACC2-T) is proposed to describe the thermo-mechanical behavior of fine-grained soils under multiple thermal cycles. Compared with TEAM model, two thermal yield limits are removed and the loading yield limits unify the thermal and loading yielding part. A dependency law with thermal accumulation parameter n_c is used to link the inner loading yield limit and the loading yield limit. Parameter n_c controls the evolution rate of the inner loading yield limit approaching the loading yield limit under thermal loading path. With such a unique dependency law and multiple plastic hardening rules, the model could well control the thermal strain accumulation rate under drained conditions and pore water pressure

buildup rate under undrained conditions. Tests on four fine-grained soils are considered to verify the proposed model. Comparison between prediction and experiment shows that ACC2-T model can well capture the thermo-mechanical behavior of soils under multiple thermal cycles.

Acknowledgements

The present work is carried out with the support of National Natural Science Foundation of China (51608188, 758201011). The authors also wish to acknowledge the support of the European Commission by the Marie Skłodowska-Curie Actions HERCULES-Towards Geohazards Resilient Infrastructure Under Changing Climates (H2020-MSCA-RISE-2017, 778360)

Notation

α_0 = parameter controlling thermal plastic behavior;

α_1 = parameter controlling thermal elastic behavior;

β = the size parameter of potential plastic surface;

λ, κ = slope of isotropic loading, reloading line respectively;

υ, ν = current void ratio, Poisson's ratio respectively;

A_d = parameter controlling the contribution of shear plastic strain;

$d\boldsymbol{\varepsilon}$, $d\boldsymbol{\sigma}$, dT = total strain, stress, temperature increment respectively;

$d\boldsymbol{\varepsilon}_{\sigma}^{e}$, $d\boldsymbol{\varepsilon}_{T}^{e}$ = stress, thermal induced elastic strain increment respectively;

$d\varepsilon_v$, $d\varepsilon_v^e$, $d\varepsilon_s^e$ = total volumetric, elastic volumetric, shear strain increment respectively;

$d\boldsymbol{\varepsilon}^p$, $d\varepsilon_v^p$, $d\varepsilon_s^p$ = plastic, plastic volumetric, plastic shear strain increment respectively;

Λ = plastic multiplier;

f_l, f_Y = Loading surface, yield surface respectively;

G, K, h = elastic shear, elastic bulk, plastic modulus respectively;

k_f, k_g = parameter controlling the shape of yield surface, plastic potential surface respectively;

M_f = stress ratio at the apex of yield surface;

M_g, M_{g0} = critical stress ratio at current, reference temperature respectively;

p', $\overline{p}'$ = current, mapping mean effective stress respectively;

p'_{cT}, p'_{c0} = pre-consolidation pressure in loading surface at current, reference temperature respectively;

$\overline{p}'_{cT}$, $\overline{p}'_{c0}$ = pre-consolidation pressure at current, reference temperature respectively;

q, $\overline{q}$ = current, mapping deviator stress respectively;

r, r_0 = reverse of OCR at current, reference temperature respectively;

s = parameter controlling the rate of evolution of the slope of the stress--strain relation;

T, T_0 = current, reference temperature respectively;

$\mathbf{D}_e$, $\mathbf{D}_{ep}$, $\mathbf{D}_{et}$ = elastic, elasto-plastic, temperature stiffness matrix respectively;

m = unit vector.

Appendix A

The consistency condition of loading surface in ACC2-T model is adopted herein:

$$\left(\frac{\partial f_I}{\partial \boldsymbol{\sigma}'}\right)^t : d\boldsymbol{\sigma}' + \frac{\partial f_I}{\partial T} dT + \frac{\partial f_I}{\partial \overline{p}'_{c0}} d\overline{p}'_{c0} + \frac{\partial f_I}{\partial r_0} dr_0 = 0 \tag{A - 1}$$

The plastic multiplier Λ and the plastic modulus h are obtained in non-isothermal condition:

$$d\boldsymbol{\varepsilon}^p = \Lambda \frac{\partial g_I}{\partial \boldsymbol{\sigma}'} \tag{A - 2}$$

$$\Lambda = -\frac{\left(\frac{\partial f_I}{\partial \boldsymbol{\sigma}'}\right)^t : d\boldsymbol{\sigma}' + \frac{\partial f_I}{\partial T} dT}{\frac{\partial f_I}{\partial \overline{p}'_{c0}} \frac{\upsilon}{\lambda - k} \overline{p}'_{c0} \frac{\partial g_I}{\partial p'} + \frac{\partial f_I}{\partial r_0} \frac{\upsilon}{\lambda - k} s(1 - r_0)\left(\frac{\partial g_I}{\partial p'} + A_d \frac{\partial g_I}{\partial q}\right)} \tag{A - 3}$$

$$h = \frac{\upsilon}{\lambda - k}\left(\frac{\partial f_I}{\partial \overline{p}'_{c0}} \overline{p}'_{c0} \frac{\partial g_I}{\partial p'} + \frac{\partial f_I}{\partial r_0} s(1 - r_0)\left(\frac{\partial g_I}{\partial p'} + A_d \frac{\partial g_I}{\partial q}\right)\right) \tag{A - 4}$$

The total strain increment is made up of mechanical elastic strain increment, thermal elastic strain increment and plastic strain increment.

$$d\boldsymbol{\varepsilon} = d\boldsymbol{\varepsilon}^e_{\sigma'} + d\boldsymbol{\varepsilon}^e_T + d\boldsymbol{\varepsilon}^p \tag{A - 5}$$

The thermal elastic strain increment $d\boldsymbol{\varepsilon}^e_T$ is defined as:

$$d\boldsymbol{\varepsilon}^e_T = -\frac{1}{3}\mathbf{m}\alpha_1 dT \tag{A - 6}$$

where **m** is the column vector with 1 at normal stress entries and 0 at shear stress entries.

By substituting Eq. A-6 into Eq. A-5, the general incremental stress-strain relation can be expressed:

$$d\boldsymbol{\sigma}' = \mathbf{D}_e d\boldsymbol{\varepsilon}^e_{\sigma'} = \mathbf{D}_e\left(d\boldsymbol{\varepsilon} + \frac{1}{3}\mathbf{m}\alpha_1 dT - d\boldsymbol{\varepsilon}^p\right) \tag{A - 7}$$

where $\mathbf{D}_e$ is the mechanical elastic matrix.

By substituting the plastic multiplier into Eq. A-7, the differential stress–strain equations can be obtained:

$$d\boldsymbol{\sigma}' = \mathbf{D}_{ep} d\boldsymbol{\varepsilon} + \mathbf{D}_{et} dT \tag{A - 8}$$

where $\mathbf{D}_{ep}$, $\mathbf{D}_{et}$ are the mechanical elasto-plastic matrix and the thermal elasto-plastic matrix, respectively.

$$\mathbf{D}_{ep} = \mathbf{D}_e - \frac{\mathbf{D}_e \dfrac{\partial g_I}{\partial \boldsymbol{\sigma}'} \left(\dfrac{\partial f_I}{\partial \boldsymbol{\sigma}'} \right)^t \mathbf{D}_e}{\left(\dfrac{\partial f_I}{\partial \boldsymbol{\sigma}'} \right)^t \mathbf{D}_e \dfrac{\partial g_I}{\partial \boldsymbol{\sigma}'} + h} \tag{A - 9}$$

$$\mathbf{D}_{et} = \frac{\mathbf{D}_e \dfrac{\partial g_I}{\partial \boldsymbol{\sigma}'} \left[-\dfrac{1}{3} \left(\dfrac{\partial f_I}{\partial \boldsymbol{\sigma}'} \right)^t \mathbf{D}_e \mathbf{m} \alpha_1 - \dfrac{\partial f_I}{\partial T} \right]}{\left(\dfrac{\partial f_I}{\partial \boldsymbol{\sigma}'} \right)^t \mathbf{D}_e \dfrac{\partial g_I}{\partial \boldsymbol{\sigma}'} + h} + \frac{1}{3} \mathbf{D}_e \mathbf{m} \alpha_1 \tag{A - 10}$$

Appendix B

Assume the soil is loaded and heated from Point A to Point B under two different loading paths I($A \to C \to B$) and II($A \to D \to B$) in Fig.5. The soil is at the initial stress state (p_0', r_0, p_{c0}', T_1) which automatically satisfies the yield condition:

$$f_{I0} = p_0' - r_0 p_{c0}' \exp\left[-\alpha_0 r_0^{n_c}\left(T_1 - T_0\right)\right] = 0 \tag{B - 1}$$

Under loading path I, the soil element is isotropically loaded to stress point C ($p_0' + \Delta p_1', r_1, p_{c1}', T_1$) at constant temperature T_1.

$$f_{I1} = p_0' + \Delta p_1' - r_1 p_{c1}' \exp\left[-\alpha_0 r_1^{n_c}\left(T_1 - T_0\right)\right] = 0 \tag{B - 2}$$

$$p_{c1}' = p_{c0}' \exp\left[\frac{\upsilon}{\lambda - \kappa}\Delta\varepsilon_{v1}^{p}\right] \tag{B - 3}$$

$$r_1 = 1 + \left(r_0 - 1\right)\exp\left[-\frac{\upsilon}{\lambda - \kappa} s \Delta\varepsilon_{v1}^{p}\right] \tag{B - 4}$$

Then the soil element is heated up to stress point B ($p_0' + \Delta p_1', r_2, p_{c2}', T_1 + \Delta T_1$) at constant mean effective stress $p_0' + \Delta p_1'$.

$$f_{I2} = p_0' + \Delta p_1' - r_2 p_{c2}' \exp\left[-\alpha_0 r_2^{n_c}\left(T_1 + \Delta T_1 - T_0\right)\right] = 0 \tag{B - 5}$$

$$p_{c2}' = p_{c1}' \exp\left[\frac{\upsilon}{\lambda - \kappa}\Delta\varepsilon_{v2}^{p}\right] = p_{c0}' \exp\left[\frac{\upsilon}{\lambda - \kappa}\left(\Delta\varepsilon_{v1}^{p} + \Delta\varepsilon_{v2}^{p}\right)\right] \tag{B - 6}$$

$$r_2 = 1 + \left(r_1 - 1\right)\exp\left[-\frac{\upsilon}{\lambda - \kappa} s \Delta\varepsilon_{v2}^{p}\right] = 1 + \left(r_0 - 1\right)\exp\left[-\frac{\upsilon}{\lambda - \kappa} s\left(\Delta\varepsilon_{v1}^{p} + \Delta\varepsilon_{v2}^{p}\right)\right] \tag{B - 7}$$

Under loading path II, the soil element is firstly heated up to stress point D ($p_0', r_3, p_{c3}', T_1 + \Delta T_1$) at constant mean effective stress p_0'.

$$f_{I3} = p_0' - r_3 p_{c3}' \exp\left[-\alpha_0 r_3^{n_c}\left(T_1 + \Delta T_1 - T_0\right)\right] = 0 \tag{B - 8}$$

$$p_{c3}' = p_{c0}' \exp\left[\frac{\upsilon}{\lambda - \kappa}\Delta\varepsilon_{v3}^{p}\right] \tag{B - 9}$$

$$r_3 = 1 + \left(r_0 - 1\right)\exp\left[-\frac{\upsilon}{\lambda - \kappa} s \Delta\varepsilon_{v3}^{p}\right] \tag{B - 10}$$

Then, the soil element is isotropically loaded to stress point B ($p_0' + \Delta p_1', r_4, p_{c4}', T_1 + \Delta T_1$)

617 at constant temperature $T_1 + \Delta T_1$.

618 $$f_{I4} = p_0' + \Delta p_1' - r_4 p_{c4}' \exp\left[-\alpha_0 r_4^{n_c}\left(T_1 + \Delta T_1 - T_0\right)\right] = 0 \quad \text{(B - 11)}$$

619 $$p_{c4}' = p_{c3}' \exp\left[\frac{\upsilon}{\lambda - \kappa}\Delta\varepsilon_{v4}^p\right] = p_{c0}' \exp\left[\frac{\upsilon}{\lambda - \kappa}\left(\Delta\varepsilon_{v3}^p + \Delta\varepsilon_{v4}^p\right)\right] \quad \text{(B - 12)}$$

620 $$r_4 = 1 + (r_3 - 1)\exp\left[-\frac{\upsilon}{\lambda - \kappa} s\Delta\varepsilon_{v4}^p\right] = 1 + (r_0 - 1)\exp\left[-\frac{\upsilon}{\lambda - \kappa} s\left(\Delta\varepsilon_{v3}^p + \Delta\varepsilon_{v4}^p\right)\right] \quad \text{(B - 13)}$$

621 Compare Eqs.B-5, B-6, B-7 and Eqs.B-11, B-12, B-13, it appears clearly that the two
622 different loading paths would reach the same final stress state, namely:

623 $$p_{c2}' = p_{c4}' \quad \text{(B - 14)}$$

624 $$r_2 = r_4 \quad \text{(B - 15)}$$

625 $$\Delta\varepsilon_{v1}^p + \Delta\varepsilon_{v2}^p = \Delta\varepsilon_{v3}^p + \Delta\varepsilon_{v4}^p \quad \text{(B - 16)}$$

626 No matter Path I or Path II is followed, the plastic volumetric strain will be equal, which
627 means that plastic volumetric strain in ACC2-T model is also loading path independent.
628
629
630
631
632
633
634
635
636
637
638
639
640
641
642

643 ## References

644 [1] Bourne-Webb PJ, Amatya B, Soga K, Amis T, Davidson C, Payne P. Energy pile
645 test at Lambeth College, London: geotechnical and thermodynamic aspects of pile
646 response to heat cycles. Géotechnique 2009;59:237-48.
647 [2] Amatya BL, Soga K, Bourne-Webb PJ, Amis T, Laloui L. Thermo-mechanical
648 behaviour of energy piles. Geotechnique 2012;62:503-19.
649 [3] Mimouni T, Laloui L. Behaviour of a group of energy piles. Canadian Geotechnical
650 Journal 2015;52:1913-29.
651 [4] Gens A, Sanchez M, Guimaraes LD, Alonso EE, Lloret A, Olivella S, et al. A full-
652 scale in situ heating test for high-level nuclear waste disposal: observations, analysis
653 and interpretation. Geotechnique 2009;59:377-99.
654 [5] Liu XC, Xiao YM, Inthavong K, Tu JY. A fast and simple numerical model for a
655 deeply buried underground tunnel in heating and cooling applications. Applied Thermal
656 Engineering 2014;62:545-52.
657 [6] Campanella R G, Mitchell J K. Influence of temperature variations on soil behavior.
658 Journal of Soil Mechanics & Foundations Div, 1968.
659 [7] Eriksson L G. Temperature effects on consolidation properties of sulphide clays.
660 International Conference on Soil Mechanics and Foundation Engineering: 13/08/1989-
661 18/08/1989. Balkema Publishers, AA/Taylor & Francis The Netherlands, 1989: 2087-
662 2090.
663 [8] Baldi G, Hueckel T, Peano A, Pellegrini R. Developments in modelling of
664 thermohydro-geomechanical behaviour of Boom clay and clay-based buffer materials
665 (volume 2). Commission of the European Communities, 1991.
666 [9] Delage P, Sultan N, Cui Y J. On the thermal consolidation of Boom clay. Canadian
667 Geotechnical Journal, 2000, 37(2): 343-354.
668 [10] Yavari N, Tang AM, Pereira JM, Hassen G. Mechanical behaviour of a small-scale
669 energy pile in saturated clay. Géotechnique 2016;66:878-87.
670 [11] Ng CWW, Shi C, Gunawan A, Laloui L. Centrifuge modelling of energy piles

671 subjected to heating and cooling cycles in clay. Géotechnique Letters 2014;4:310-6.
672 [12] Hueckel T, Pellegrini R. Thermoplastic modeling of undrained failure of saturated
673 clay due to heating. Soils and Foundations, 1991, 31(3): 1-16.
674 [13] Hueckel T, Baldi G. Thermoplasticity Of Saturated Clays - Experimental
675 Constitutive Study. J Geotech Eng-Asce 1990;116:1778-96.
676 [14] Hueckel T, Borsetto M. Thermoplasticity Of Saturated Soils And Shales:
677 Constitutive equations. J Geotech Eng-Asce 1990;116:1765-77.
678 [15] Robinet JC, Rahbaoui A, Plas F, Lebon P. A constitutive thermomechanical model
679 for saturated clays. Engineering Geology 1996;41:145-69.
680 [16] Cui Y J, Sultan N, Delage P. A thermomechanical model for saturated clays.
681 Canadian Geotechnical Journal, 2000, 37(3): 607-620.
682 [17] Graham J, Tanaka N, Crilly T, Alfaro M. Modified Cam-Clay modelling of
683 temperature effects in clays. Canadian Geotechnical Journal 2001;38:608-21.
684 [18] Abuel-Naga HM, Bergado DT, Bouazza A, Ramana GV. Volume change behaviour
685 of saturated clays under drained heating conditions: experimental results and
686 constitutive modeling. Canadian Geotechnical Journal 2007;44:942-56.
687 [19] Yao YP, Zhou AN. Non-isothermal unified hardening model: a thermo-elasto-
688 plastic model for clays. Géotechnique 2013;63:1328-45.
689 [20] Laloui L, François B. ACMEG-T: soil thermoplasticity model. Journal of
690 engineering mechanics, 2009, 135(9): 932-944.
691 [21] Hong PY, Pereira JM, Cui YJ, Tang AM. A two-surface thermomechanical model
692 for saturated clays. International Journal for Numerical and Analytical Methods in
693 Geomechanics 2016;40:1059-80.
694 [22] Hong PY, Pereira JM, Tang AM, Cui YJ. On some advanced thermo-mechanical
695 models for saturated clays. International Journal for Numerical and Analytical Methods
696 in Geomechanics 2013;37:2952-71.
697 [23] Demars K R , Charles R D . Soil volume changes induced by temperature cycling.
698 Canadian Geotechnical Journal, 2011, 19(2):188-194.

699 [24] Plum R L, Esrig M I. Some temperature effects on soil compressibility and pore
700 water pressure. Special Report-Highway Research Board, 1969 (103): 231.
701 [25] Di Donna A, Laloui L. Response of soil subjected to thermal cyclic loading:
702 Experimental and constitutive study. Engineering Geology 2015;190:65-76.
703 [26] Ng CWW, Shi C, Gunawan A, Laloui L, Liu HL. Centrifuge modelling of heating
704 effects on energy pile performance in saturated sand. Canadian Geotechnical Journal
705 2015;52:1045-57.
706 [27] Vega A, McCartney JS. Cyclic heating effects on thermal volume change of silt.
707 Environmental Geotechnics 2015, 2: 257-68.
708 [28] Zhou C, Fong KY, Ng CWW. A new bounding surface model for thermal cyclic
709 behaviour. International Journal for Numerical and Analytical Methods in
710 Geomechanics 2017;41:1656-66.
711 [29] Ma QJ, Ng CWW, Masin D, Zhou C. An approach for modelling volume change
712 of fine-grained soil subjected to thermal cycles. Canadian Geotechnical Journal
713 2017;54:896-901.
714 [30] Coussy, O. (2004). Poromechanics, John Wiley and Sons, Ltd.
715 [31] McDowell GR, Hau KW. A generalised Modified Cam clay model for clay and
716 sand incorporating kinematic hardening and bounding surface plasticity. Granular
717 Matter 2004;6:11-6.
718 [32] Zhang S, Leng W, Zhang F, et al. A simple thermo-elastoplastic model for
719 geomaterials. International Journal of Plasticity, 2012, 34: 93-113.
720 [33] Collins I F , Houlsby G T . Application of thermomechanical principles to the
721 modelling of geotechnical materials. Proceedings of the Royal Society A: Mathematical,
722 Physical and Engineering Sciences, 1997, 453(1964):1975-2001.
723 [34] Lebon, Georgy, Jou, et al. Understanding non-equilibrium thermodynamics. 2008.
724 [35] B. Spang, Excel add-in for properties of water and steam in si-units, available from
725 http://www.cheresources.com/ iapwsif97.shtml, 2002 (2002).
726 [36] Yao Y P , Sun D A , Matsuoka H . A unified constitutive model for both clay and

sand with hardening parameter independent on stress path[J]. Computers & Geotechnics, 2008, 35(2):210-222.
[37] Yao Y P , Sun D A , Luo T . A critical state model for sands dependent on stress and density[J]. International Journal for Numerical and Analytical Methods in Geomechanics, 2004, 28(4): 323-337.
[38] Lê T. Comportement thermo-hydro-mécanique de l'argile de boom. PhD Thesis, École Nationale des Ponts et Chaussées, France 2008.
[39] Borja R I, Tamagnini C, Amorosi A. Coupling plasticity and energy-conserving elasticity models for clays. Journal of Geotechnical and Geoenvironmentol Engineering, 1997, 123(10): 948-957.
[40] Pastén C, Castillo E, Chong S H. Thermo-mechanical ratcheting in soil–structure interfaces. Acta Geotechnica, 2019, 14: 1561–1569.
[41] Zymnis, D M, Whittle A J, Cheng X. Simulation of long-term thermo-mechanical response of clay using an advanced constitutive model. Acta Geotechnica. 2019, 14: 295–31.

LIST OF TABLES

Table.1 Model parameters of different fine-grained soils

Parameters	κ	λ	$\overline{p}'_{c0,0}$(kPa)	$r_{0,0}$	v	α_0 ($^oC^{-1}$)	α_1($^oC^{-1}$)	s	T_0(^oC)	n_c	M_{g0}	M_f	A_d	k_f	k_g
Boom clay[8]	0.02	0.18	6000	0.33	-	5×10^{-3}	5×10^{-5}	8	21.5	-1	0.67	0.67	0.1	0.7	0.9
Geneva clay[25]	0.017	0.062	125	1	0.3	5.2×10^{-3}	1.5×10^{-5}	12	20	3.5	0.94	0.94	0.1	1.1	1.1
Bonny silt[27]	0.011	0.075	1200	*	0.3	1.6×10^{-3}	3.5×10^{-5}	10	18	4	1.3	1.3	0.2	1.1	1.1
Pontida clay[12]	0.016	0.103	2500	1	-	3.5×10^{-3}	5×10^{-5}	10	23	1	-	-	-	-	-

‘-’ means the parameters are irrelevant to the simulations in this study.

‘*’ means different data are mentioned in this study.

List of Figure Captions

condition: (a) comparison between ACC2-T model with n_c =3.5 (best fit) and TEAM model; (b) ACC2-T model with n_c =0 and n_c=10; (c) volumetric strain increment due to each thermal cycle by ACC2-T model

Fig.11 Thermal cyclic behaviors of Bonny silt with different OCRs under drained condition

Fig.12 Excess pore water pressure accumulation of Pontida clay due to thermal cycles under undrained condition: (a) ACC2-T model; (b) TEAM model

Fig.13 Correlation between thermal accumulation parameter n_c and plasticity index I_p

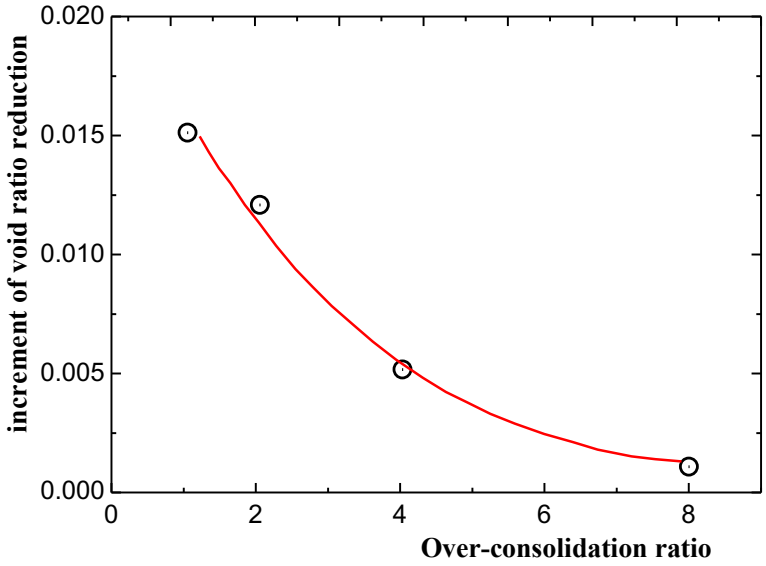

Fig.1 Permanent reduction in void ratio due to temperature cycles versus over-consolidation ratio (replotted from Demars and Charles [23])

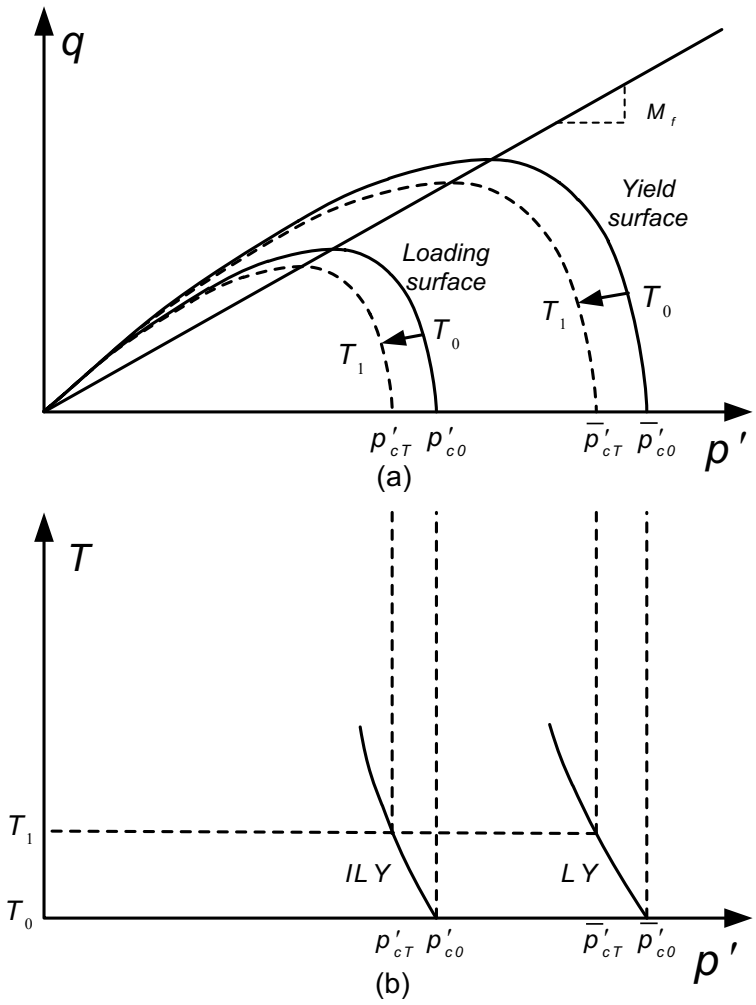

Fig.2 Yield locus in (a): (p', q) plane at two different temperatures (with $T_1 > T_0$) and (b): two loading yield limits *ILY* and *LY* in (p'-T) plane.

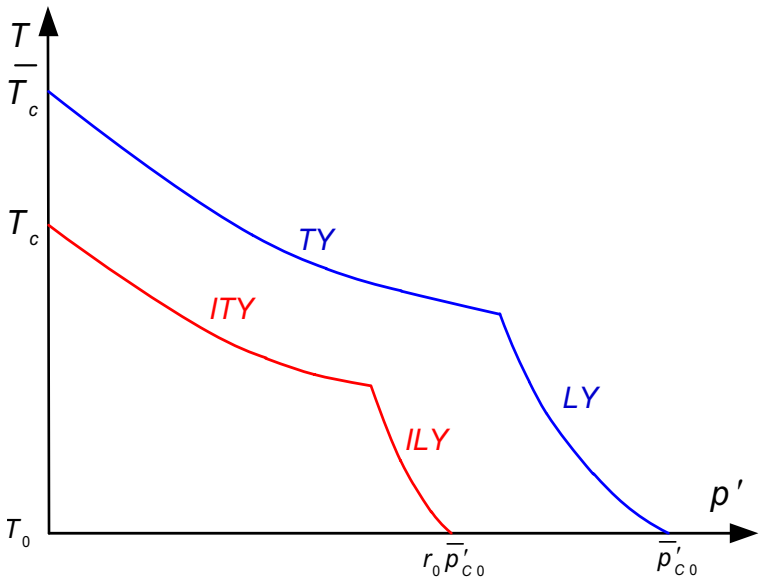

(a)

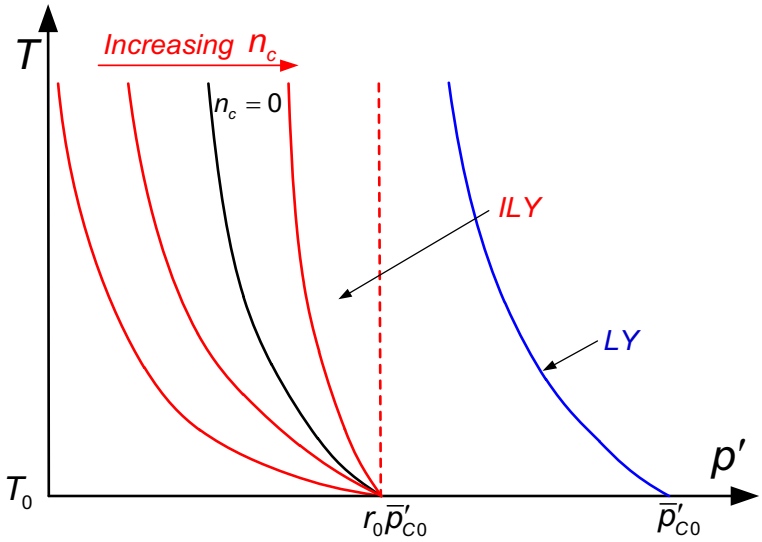

(b)

Fig.3 Yield limits in (p', T) plane: (a) TEAM Model (b) ACC2-T Model

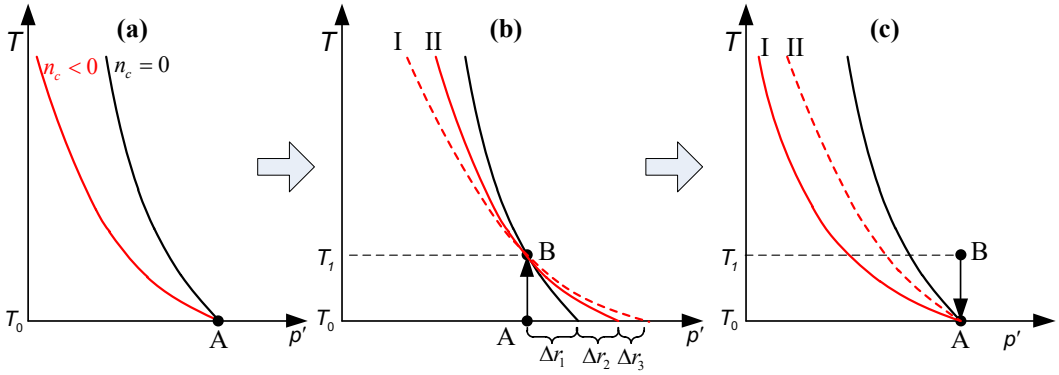

Fig.4 Evolution of yield limits in (p', T) plane during one heating and cooling cycle

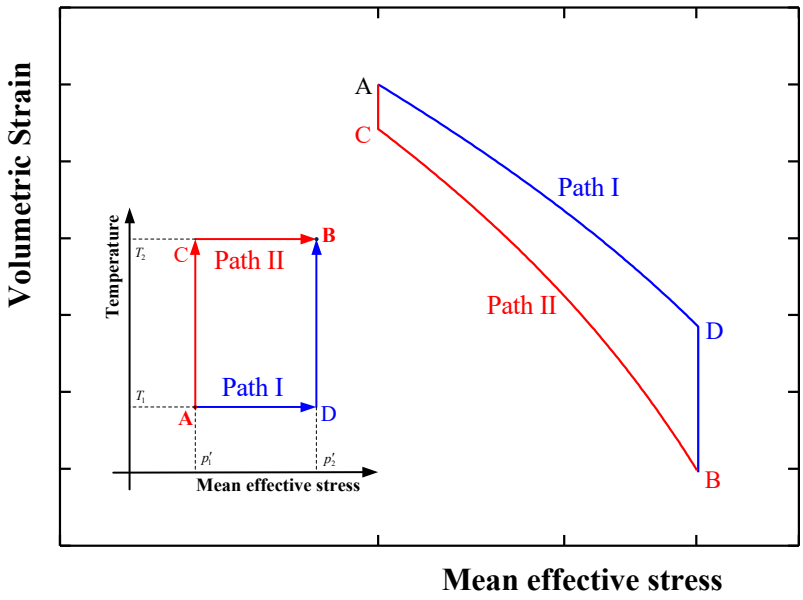

Fig.5 Predicted response of two loading paths in mean effective stress and temperature plane

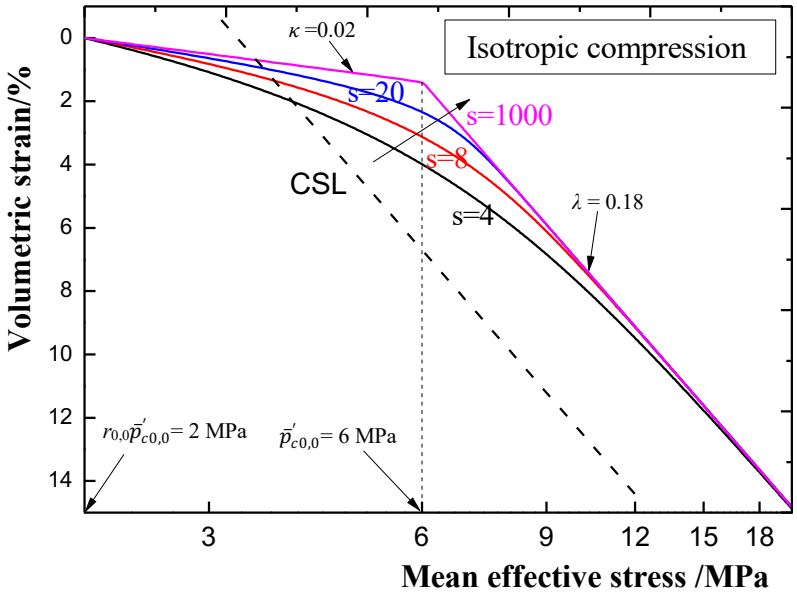
Isotropic compression
κ =0.02
s=20
s=1000
s=8
CSL
s=4
λ = 0.18
$r_{0,0}\bar{p}'_{c0,0}$= 2 MPa
$\bar{p}'_{c0,0}$= 6 MPa
Volumetric strain/%
Mean effective stress /MPa
0
2
4
6
8
10
12
14
3
6
9
12
15
18

(a)

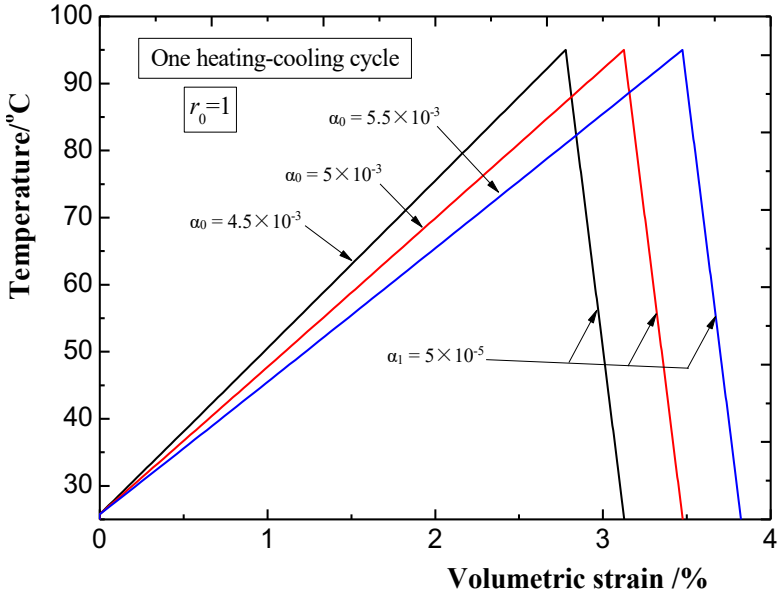
One heating-cooling cycle
r_0=1
$\alpha_0 = 5.5\times10^{-3}$
$\alpha_0 = 5\times10^{-3}$
$\alpha_0 = 4.5\times10^{-3}$
$\alpha_1 = 5\times10^{-5}$
Temperature/°C
Volumetric strain /%
100
90
80
70
60
50
40
30
0
1
2
3
4

(b)

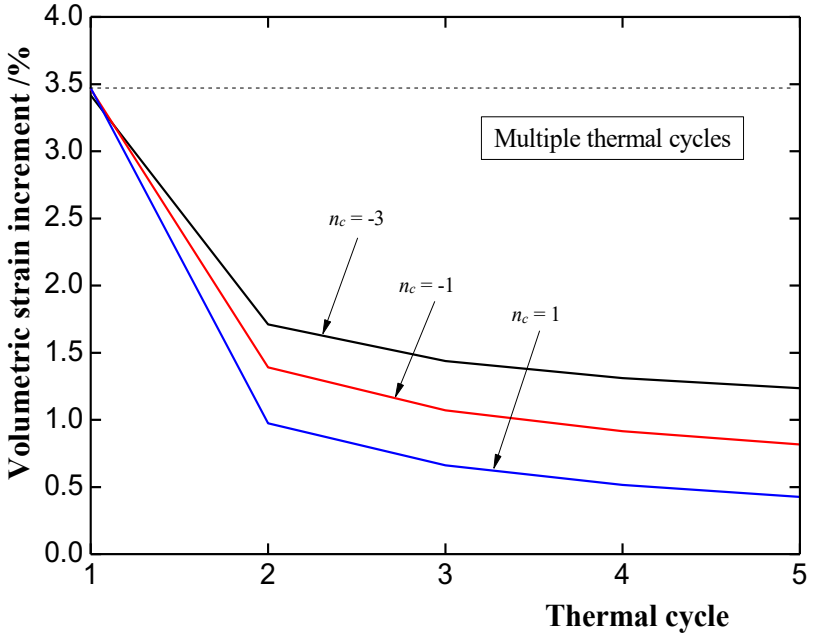

(c)

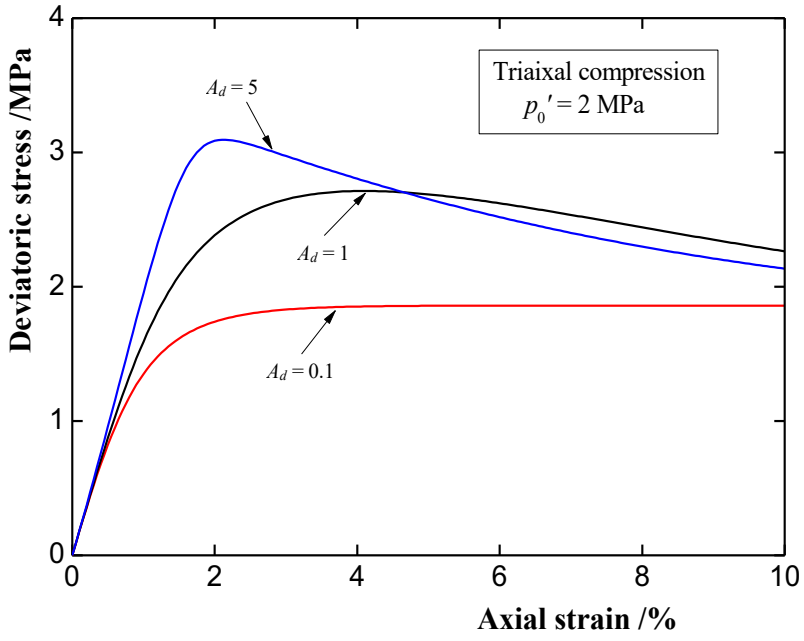

(d)

Fig.6 Calibration process of ACC2-T model on set of material parameters for Boom clay: (a) isotropic compression test; (b) one heating-cooling cycle at normal consolidated state; (c) multiple thermal cycles; (d) triaxial compression test at over-consolidated state

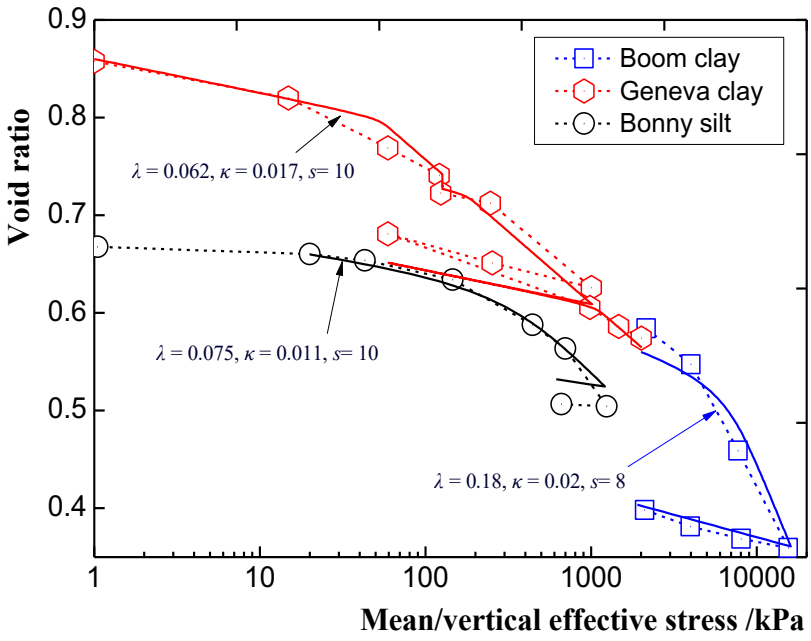

Fig.7 Isotropic/one-dimensional compression tests of Boom clay, Geneva clay and Bonny silt

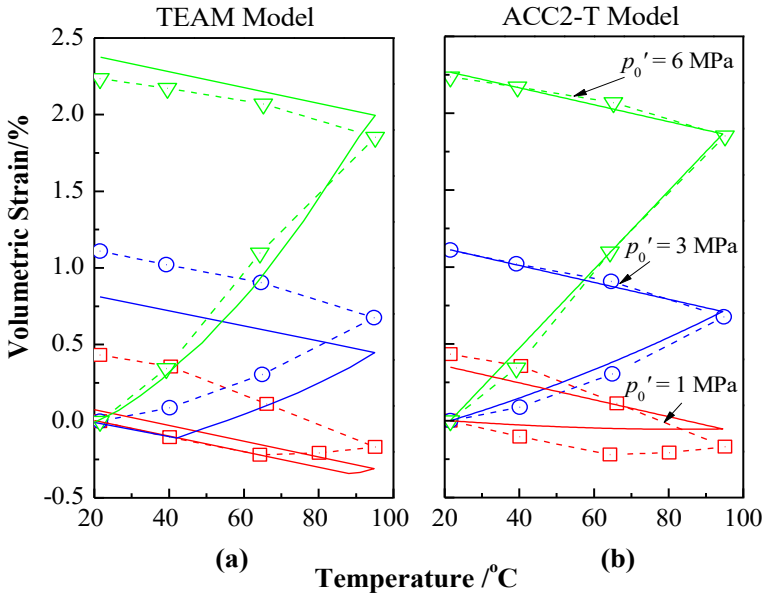

Fig.8 Volumetric strain change of Boom clay due to one heating and cooling cycle with different mean effective stresses: (a) TEAM model (b) ACC2-T model

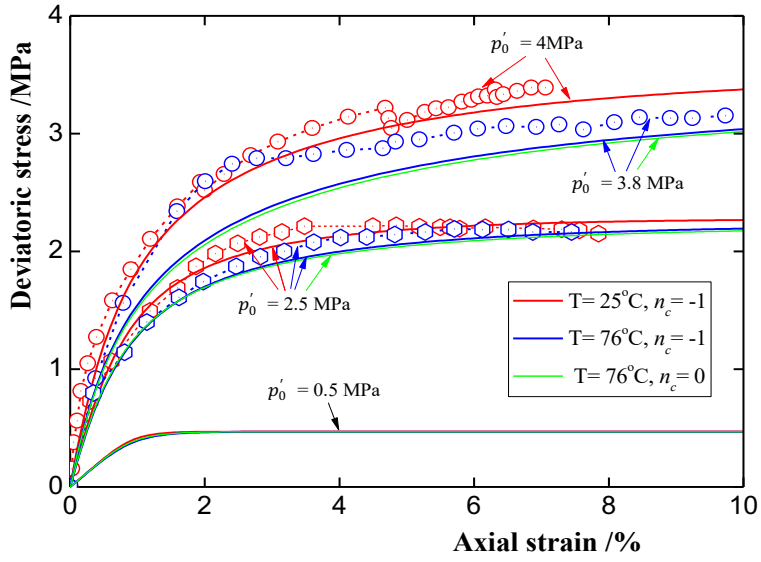

(a)

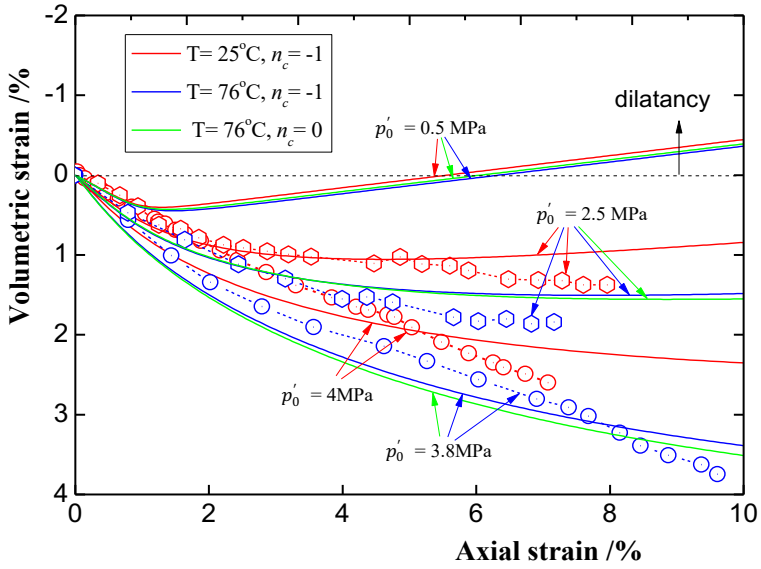

(b)

Fig. 9 Triaxial drained behaviors of Boom clay at room temperature 25 °*C* and high temperature 76 °*C*: (a) deviatoric stress vs axial strain; (b) volumetric strain vs axial strain;

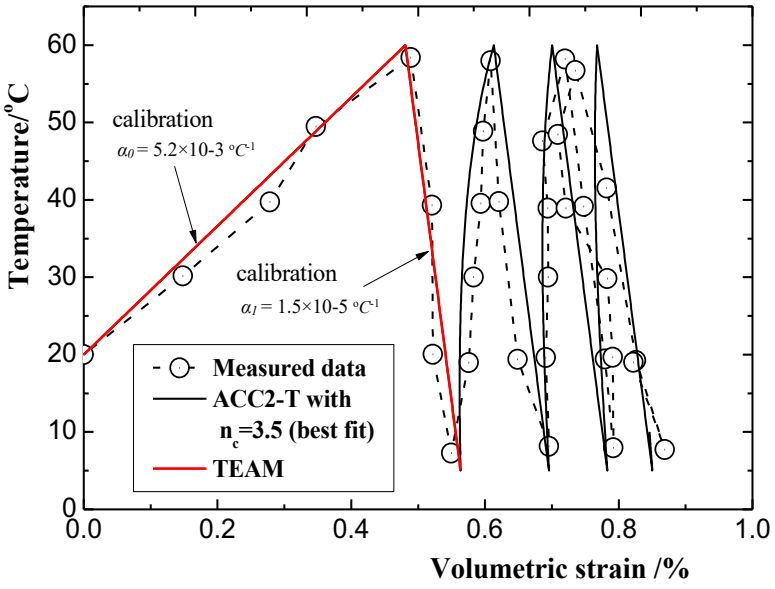
Temperature/°C
Volumetric strain /%
calibration
α_0 = 5.2×10-3 °C-1
calibration
α_1 = 1.5×10-5 °C-1
Measured data
ACC2-T with
n_c=3.5 (best fit)
TEAM

(a)

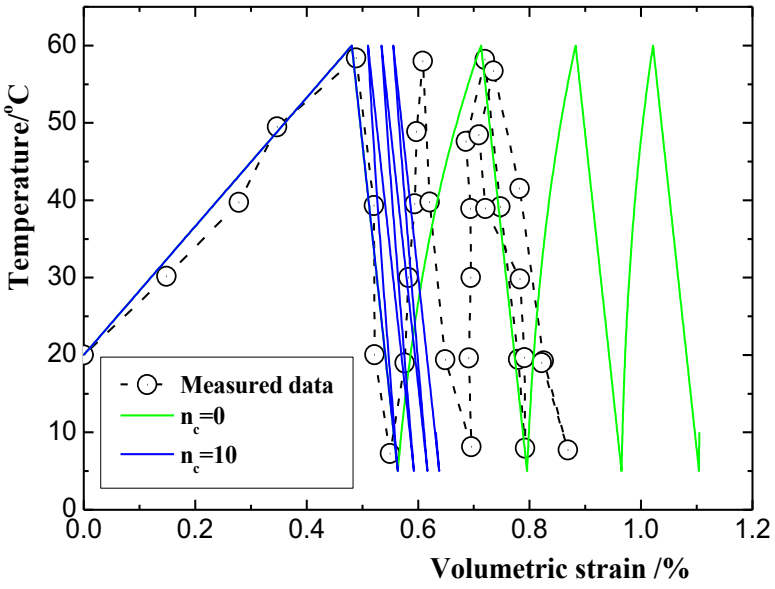
Temperature/°C
Volumetric strain /%
Measured data
n_c=0
n_c=10

(b)

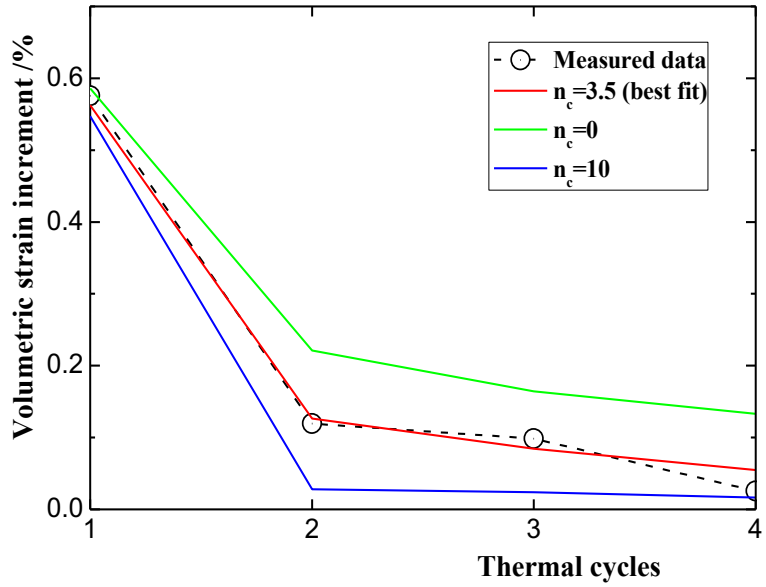

(c)

Fig.10 Thermal cyclic behaviors of normal consolidated Geneva clay under drained condition: (a) comparison between ACC2-T model with n_c=3.5 (best fit) and TEAM model; (b) ACC2-T model with n_c=0 and n_c=10; (c) volumetric strain increment due to each thermal cycle by ACC2-T model

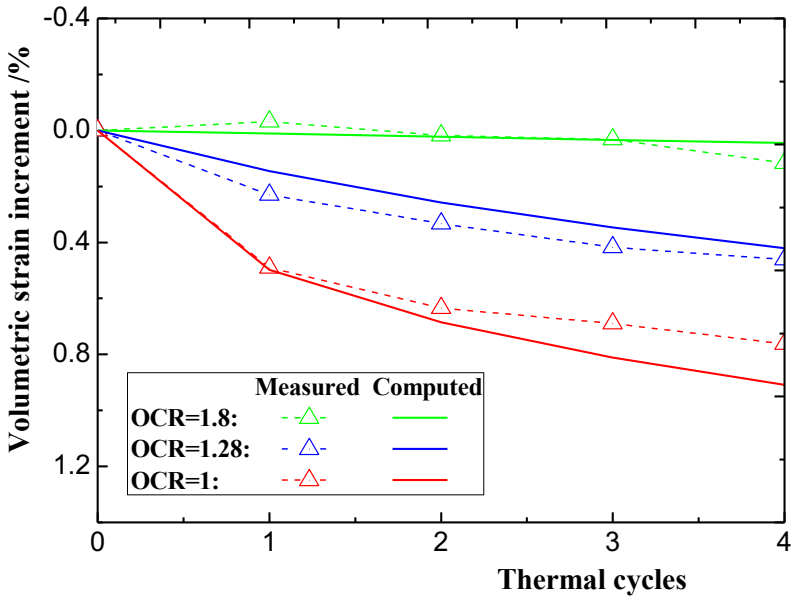

Fig.11 Accumulated strain behavior of Bonny Silt with different OCRs under drained condition

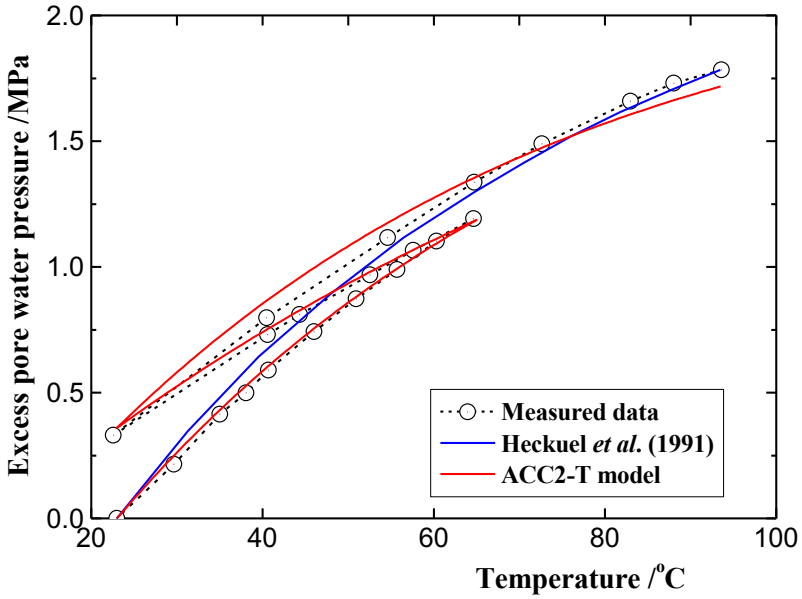

(a)

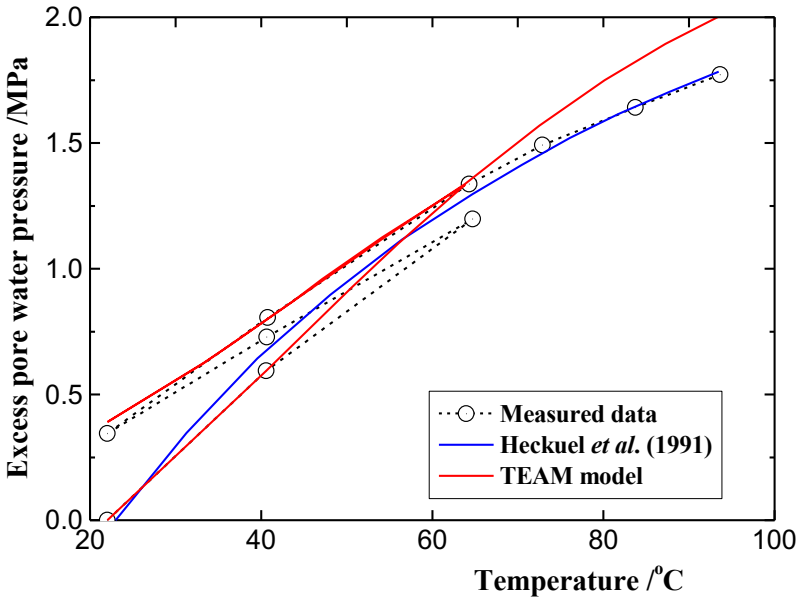

(b)

Fig.12 Excess pore water pressure accumulation of Pontida clay due to thermal cycles under undrained condition: (a) ACC2-T model; (b) TEAM model

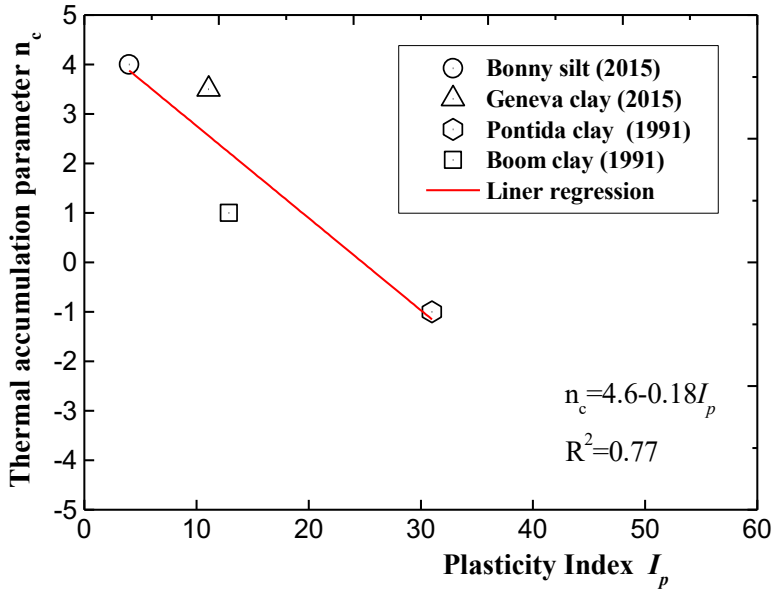

Fig.13 Correlation between thermal accumulation parameter n_c and plasticity index I_p